Chapter 6.

The Dissociation Reaction of Acetylacetone

In Section 5.6, the ground-state structure of enolic acetylacetone as determined by UED was described. It was shown that the structure was actually of C_s symmetry and not of C_{2v} symmetry as supposed by some previous studies. The C_{2v} symmetric model had been favored due to the presence of an intramolecular "resonance-assisted hydrogen bond" in the enol tautomer.[1] Beyond the ground-state controversy, however, acetylacetone was also studied with UED in order to determine its excited state structural dynamics by harnessing the real power of picosecond time-resolved electron diffraction. This chapter is based on the published communication of the results of this experiment (see Ref. 2).

6.1 Spectroscopic background

While the nature of the ground-state structure is now resolved, less is known about the excited states and their reactions. The ultraviolet spectrum of vapor-phase acetylacetone shows two very weak nπ* bands at about 3.57 and 4.04 eV.[3] The temperature (and tautomeric ratio) dependence of the spectrum assigns the 4.04 eV (~34,000 cm^{-1}) band to the nπ* of the keto. A broad structureless absorption that peaks at 4.70 eV (38020 cm^{-1}) is assigned to the first ππ* transition (S_2 state) of the enol tautomer.[3,4] Rydberg absorptions are seen to rise strongly at ~52000 cm^{-1}.[4] Emission from acetylacetone is not known.

In xenon matrices, irradiation by UV light (Hg arc, $\lambda > 230$ nm) triggers the appearance of free O–H stretching bands in the IR spectrum.[5] This change is believed to be caused by isomerization of acetylacetone by rotation about one of the single bonds such that the intramolecular hydrogen bond is broken. The terminology used is "chelated" when referring to the lowest energy, H-bonded isomer and "non-chelated" for all isomers where the H-bond is broken. No carbon monoxide is detected which the authors cite as evidence for a lack of fragmentation. There is no change in the keto signal signifying two points – keto is not reacting with the light (little absorption) and enol is not tautomerizing with the excitation. Warming of the matrix after the isomerization eliminates the free OH stretch band as the original chelated enol is restored.[5] When acetylacetone embedded in an argon matrix and excited with UV irradiation (Hg arc) the isomerization reaction was observed and further characterized with the assistance of DFT calculations.[6] Various non-chelated enols were identified by their IR spectra.

Furthermore, a rise in the keto tautomer population was observed if excitation wavelengths were < 280 nm.[6] Results of UV excitation of acetylacetone in nitrogen matrices are similar in that isomerizations are observed and different in that no keto tautomer was found.[7] A reduction in the population of the chelated enol in hydrocarbon solution after 254 nm irradiation was thought to be tautomerization. The signal from the parent chelated enol recovers with time. An intermediate between chelated enol and the keto tautomers is thought to be a non-chelated enol species.[8]

The gas phase shows a different set of reactions. OH (hydroxyl) radical was detected after UV excitation of acetylacetone in a supersonic jet. Laser-induced fluorescence (LIF) of the fragment indicated that it is vibrationally cold. Excitation wavelengths varied from 266 to 310 nm.[9] Further exploration of the OH rotational states indicates low level rotational excitation. A statistical kinetic model and the authors' own supposition tentatively predicts a mechanism through the triplet state with an exit barrier where their calculations are consistent with the OH energy partitioning.[10] This is supported by further work on OH loss from acetylacetone studied with 248, 266, and 193 nm excitation.[11] The two shortest wavelengths excite into S_2 $\pi\pi^*$ and the latter into a Rydberg state. OH fragment was spawned by all excited states studied. Using nanosecond pulses, it is found that most OH is formed within the duration of the pulse, making the rate $>10^8$ s^{-1}. A secondary OH channel rising in 800 ns is also observed. Their hybrid model predicts an exit barrier consistent with fragmentation from the T_1 $\pi\pi^*$ state with most available energy is partitioned into the translational energy of the fragments.[11] Before UED, ultrafast studies had not been performed on this molecule.

6.2 Experimental settings and notes

The UED apparatus was mostly as described in Chapter 3. The major difference was that the translation stage governing the delay was positioned in the beam path that generates the electrons rather than in the excitation laser path. This affected the data by slightly altering the center positions of the diffraction images – which had to be carefully determined for each datum. Some further settings for this experiment specifically differed from those already described and are noted in Chapter 3. The electron pulse had horizontal ($w_{horizontal}$) and vertical ($w_{vertical}$) FWHM of approximately 260 and 350 μm, respectively, and contained about 22000 electrons. This translates to a temporal pulsewidth (τ_e) of ~2 ps. The pump laser beam width was not measured but taken to be 350 μm based on the focal length of the focusing lens. The molecular beam width was measured; w_m = 324 μm. Experimental time-zero was calibrated using the lensing arising from the multi-photon ionization of CF_3I gas.

The molecular sample was introduced into the chamber through a nozzle maintained at 428 K. Acetylacetone (2,4-pentanedione) was purchased from Aldrich (>99.0%) and degassed before use by three cycles of the freeze-pump-thaw procedure. Detector background was collected, as was diffraction data for carbon dioxide, xenon, ground state acetylacetone, and time-resolved acetylacetone. The time points collected were: –77, –27, 13, 18, 23, 28, 33, 43, 73, 98, 123, 173, 223, 423, 823, and 1273 ps. These data were collected with a neutral-density filter that permitted only 10 % transmission of the pump laser light. A second set of time-resolved data were collected with no filter at –77, 98, and 1273 ps time points.

The starting geometries of ground-state molecules needed for structural analysis were obtained by quantum chemical (DFT) calculations at the B3LYP/6-311G(d,p) level. Calculations of excited states were performed at the CASSCF(10,9)/6-31G(d,p) level.

The detector range 38–185 pixels (s = 2.93 to 14.14 $Å^{-1}$) was used. A camera length of 13.49 cm was obtained from the fit with CO_2 data. The scale factor used for the time-resolved data was $1/\lambda = 2.085$ taken from a fit of the ground state structure to the –100 ps time point. The parent species for the reaction was modeled with the DFT structure of the C_s chelated enol. The DFT structure was used over the UED refined structure since ground state diffraction data are often subject to systematic errors that are subtracted out in the difference data (e.g., residual background gas scattering).

6.3 Results and discussion

The time-resolved difference ratio images are shown in Figs. 6-1 and 6-2. Note the slow growth in intensity over time signifying – even without any quantitative analysis – that the rate of product formation is slow. Of course, the presence of diffraction rings at all in the difference ratio patterns means structural change is occurring. The comparison between filtered and unfiltered data in Fig. 6-3 is useful in that the similarities confirm either 1) the lack of multi-photon effects or 2) the same reaction pathways regardless of excitation energy.

Excitation of acetylacetone at 266.7 nm results in population of the S_2 $\pi\pi^*$ excited state near the peak of that band. In order to get a rough idea of the reaction pathways occurring after the excitation, the time-resolved diffraction (referenced with the –77 ps

time point) data are compared with theoretical diffraction data generated using calculated structures of possible products as noted in the literature. Based on previous spectroscopy experiments[3,4] it is taken that the keto tautomer does not absorb significantly at 266.7 nm and is thus subtracted out when difference data are made. Table 6-1 lists some of the possible products and the energies relative to the parent chelated (CCC) enol. T_B^{Max} values are the vibrational temperatures calculated assuming all excess energy is partitioned into the normal modes as described in Section 4.5.4. It should be noted that the energies predicted by DFT for OH loss are outside of the possible excitation. Since OH loss has been found after excitation of acetylacetone at 266.7 nm, it is clear that the DFT energies are overestimated. The T_B^{Max} for these products is taken to be 428 K, the initial (nozzle) temperature. Fig. 6-4 shows the schematic diagrams of the possible isomerization pathways and Fig. 6-5 the other possible reaction products.

Table 6-1. Energies and T_B^{Max} of possible reaction products

Product	ΔE (kcal/mol)	T_B^{Max} (K)
enol CCC	0.0	2256
enol CCT	14.2[a]	2000†
enol CTC	11.7[a]	2000†
enol CTT	16.0[a]	2000†
enol TCC	17.2[a]	2000†
enol TTC	12.8[a]	2000†
enol TCT	15.4[a]	2000†
enol TTT	18.9[a]	2000†
keto tautomer	5.0	2175
OH-loss, CC	115.1	428*
OH-loss, CT	117.3	428*
OH-loss, TC	117.5	428*
OH-loss, TT	115.0	428*
Acetyl-loss	104.0	617
Methyl-loss, Norrish	81.7	1145

a) Energies are taken from Ref. 6 and based on DFT calculations at the B3LYP/6-31G(d) level.

*) T_B^{Max} set at nozzle temperature (see text)

†) Temperatures estimated since normal mode frequency calculations were unavailable.

Using the DFT structure of the chelated enol and the structures of the various possible reaction products, theoretical $\Delta sM(s)$ were calculated and compared with the experimental $\Delta sM(s)$ at the +1273 ps time point (t_{ref} = –77 ps) (all refinements herein were conducted on of the unfiltered data unless otherwise noted). Figs. 6-6 and 6-7 show the $\Delta sM(s)$ and $\Delta f(r)$ comparisons for the possible isomerization pathways. Each possible product structure is modeled at T_B^{Max} where available – the temperatures listed in Table 6-1 were used to calculate *l* values. Inspection of the curves of the isomerization pathways makes clear some common inconsistencies between theory and experiment. In the $\Delta sM(s)$ curves, there is a peak in the data at s ~8 Å^{-1} that is completely out of phase with the peak in the theoretical curves of all isomers. In the $\Delta f(r)$ curves, the major difference is in the region of direct bond lengths: 1 Å < r < 2 Å. Although it is a crude

assumption, at this point it is reasonable to believe that the structure represented in the data at +1273 ps has experienced a direct bond breakage relative to the parent enol.

Table 6-2. The fraction fits of the various product channels

Product	Old program (Uedana)			New program (UED_2004)		
	fraction (%)	χ^2	*R*	fraction (%)	χ^2	*R*
enol CCC	22.77	36.623	1.160	23.60	38.346	1.128
enol CCT	14.76	35.455	1.070	15.01	35.223	1.056
enol CTC	17.77	36.549	1.103	17.96	36.388	1.096
enol CTT	11.82	40.770	1.260	11.92	40.573	1.255
enol TCC	20.08	30.374	0.902	20.25	30.215	0.897
enol TTC	18.50	35.383	1.069	18.80	35.182	1.055
enol TCT	17.11	32.652	0.980	17.38	32.450	0.968
enol TTT	12.36	38.637	1.174	12.46	38.408	1.170
enol CCC + keto mix	9.63+9.63	15.462	0.508	12.71+12.71	19.851	0.439
OH-loss, CC	14.83	19.312	0.619	14.93	19.092	0.613
OH-loss, CT	12.05	23.580	0.722	12.20	23.294	0.713
OH-loss, TC	17.02	15.654	0.533	16.76	15.673	0.535
OH-loss, TT	15.05	18.582	0.603	15.18	18.410	0.598
Acetyl-loss	15.28	21.945	0.680	15.93	22.793	0.698
Methyl-loss, Norrish	15.12	39.917	1.222	15.50	38.516	1.153

Error bars (3σ) for the fractions are about 20% of the tabulated values.

Fig. 6-5 shows schematics of possible products resulting from either tautomerization or fragmentation. The tautomerization pathway assumes that excitation of the enol followed by internal conversion to the ground state forms a 1:1 mixture of vibrationally hot enol and keto tautomers: the enol tautomer at 2256 K and the keto tautomer at 2175 K. In principle, since the keto tautomer is chiral, the ratio should be 1:2, but the property is ignored here. The loss of the OH group may form several isomers of the 2-penten-4-on-3-yl radical, which were all tested for their possibility as a reaction product. Fig. 6-8 and 6-9 show the comparison between experimental and theoretical $\Delta sM(s)$ and $\Delta f(r)$ curves for the structures in Fig. 6-5. As with the test fits of isomers of the parent, inspection of these test-fit curves tells much about the nature of the product structure. In all $\Delta sM(s)$ curves in Fig. 6-8, the peak at $s \sim 5.5$ Å^{-1} does not match well. The methyl loss channel shows a number of mismatched peaks. The hot ground state

mixture models the data well. Fig. 6-9 shows the curves for the various rotamers of the OH loss products. Other than the CT isomer, the others are all reasonable fits to the data and will be further considered and discussed. Although some isomerization of the chelated (H-bond intact) enol into non-chelated enol in matrices[5-7] and in solution[8] has been studied, the poor match between this model and the data indicates that the pathway is not significant in the isolated reaction.

The visual comparison provides an intuitive way of choosing an appropriate starting point for structural refinement. The test fits are also accompanied by quantitative statistical information, χ^2 and R, which are listed in Table 6-2. Table 6-2 also contains the fraction of reaction that produces the minimum χ^2 value as well as a comparison between the results of old and new analysis programs (see Section 4.8). Based on these measures, the most favorable models of product structure are the hot ground-state mixture and the TC isomer of the OH loss channel.

Structural refinement was conducted using both possibilities. For the hot ground-state mixture, structural refinement had lukewarm results – when molecules are at such a high temperature their contributions to the diffraction signal become heavily washed-out and structural changes in the model structure have a smaller effect on the fit. Consequently, refinement of the hot keto and enol structures showed no large geometric changes. However, a big change was experienced when the fraction of enol and keto products was allowed to float. Enol was eliminated and the entire product fraction became dominated by the hot keto structure. This was taken as the proof that the reaction was not a correct model of the experiment (see above comment on proper fractional

proportions). Superior structural refinement results were obtained with a model (z-matrix) for the TC rotamer of the 2-penten-4-on-3-yl radical resulting from the OH loss channel. Combinations of the previously mentioned channels were tested by comparing the data with mixtures of several theoretical models. This produced slightly improved fits (as more degrees of freedom are present). However, since the OH loss channel always remained the dominant component, structural refinement could be carried out successfully with this channel being the sole reaction pathway.

C1						
C2	C1	r1				
C3	C2	r2	C1	a1		
C4	C3	r3	C2	a2	C1	d1
C5	C4	r4	C3	a3	C2	d2
O6	C2	r5	C1	a4	C3	d3
O7	C4	r6	C5	(360-a3)/2	C3	d4
H8	C1	r7	C2	a5	C3	d5
H9	C1	r8	C2	a6	H8	d6
H10	C1	r9	C2	a7	H8	d7
H11	C3	r10	C2	a8	C4	d8
H12	O6	r11	C2	a9	C1	d9
H13	C5	r12	C4	a10	C3	d10
H14	C5	r13	C4	a11	H13	d11
H15	C5	r14	C4	a12	H13	d12

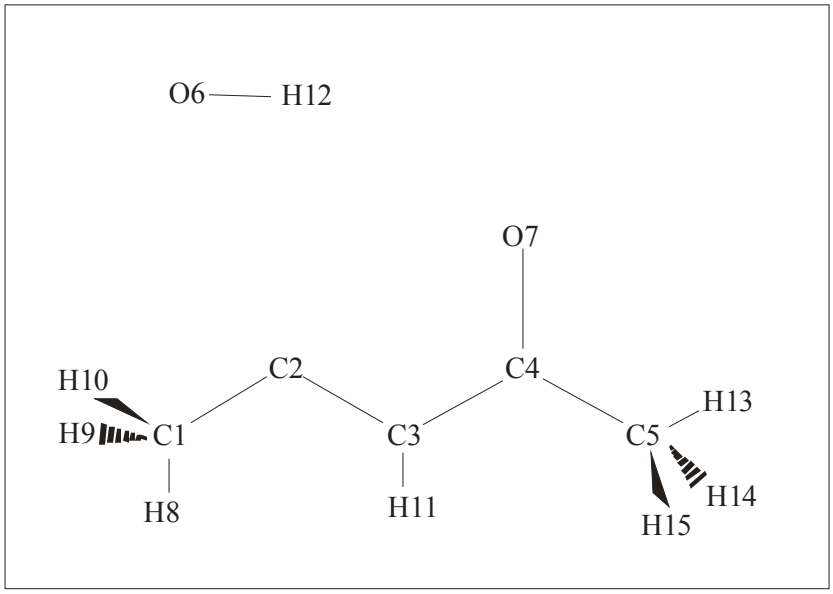

The structure of 2-penten-4-on-3-yl was refined while fixing all hydrogen-related parameters at their DFT determined values. The O–H distance of the OH radical was also fixed at the DFT value. The one dependency in the above z-matrix maintains that the C4–O7 bond bisects the C3C4C5 angle (marked in Table 6-3 with an asterisk). The independence of the two radicals in one z-matrix was accomplished by setting the distance between them (r5) to 100 Å. The final structure is listed in Table 6-3 along with the corresponding values given by DFT.

Table 6-3. The structure of the OH-loss channel products

Parameters	UED	DFT
r(C1-C2)	1.542 ± 0.023	1.462
r(C2-C3)	1.304 ± 0.025	1.316
r(C3-C4)	1.482 ± 0.023	1.499
r(C4-C5)	1.564 ± 0.047	1.519
r(C4-O7)	1.202 ± 0.017	1.212
r(C1-H8)	-	1.101
r(C1-H9), *r*(C1-H10)	-	1.095
r(C3-H11)	-	1.096
r(C5-H13)	-	1.089
r(C5-H14), *r*(C5-H15)	-	1.095
r(O6-H12)	-	0.975
a(C1-C2-C3)	139.4 ± 5.9	141.5
a(C2-C3-C4)	121.9 ± 1.7	123.8
a(C3-C4-C5)	110.1 ± 2.8	115.4
a(C5-C4-C7)	125.0*	121.9
a(H8-C1-C2)	-	116.6
a(H9-C1-C2), *a*(H10-C1-C2)	-	110.9
a(H11-C3-C2)	-	119.5
a(H13-C5-C4)	-	109.6
a(H14-C5-C4), *a*(H15-C5-C4)	-	110.4
φ(C2-C3-C4-C5)	–159.8 ± 14.2	180.0
φ(H8-C1-C2-C3)	-	0.3
φ(H13-C5-C4-C3)	-	–180.0

The refined covalent bond distances and angles show some deviations from the equilibrium structures predicted by quantum chemical calculations. The bonds connecting the methyl groups to the remainder of the carbon skeleton, *r*(C1–C2) and *r*(C4–C5), are longer by 0.080 and 0.045 Å, respectively. The reason for this deviation is not clear. Like any other experimental/theoretical disagreement, either it's the experiment, the theory, or something unforeseen. The possibility that the bond length is effectively lengthened by vibration or rotation that is not modeled by UED methodology cannot be ruled out. Also at variance from theory, the acetyl group is rotated out of the plane of the molecule by ~20° instead of being coplanar. This indicates that the radical is able to rotate around the C–C single bond. The fitted value reflects an average over all the rotations present in the products.

Structurally, due to the loss of intramolecular hydrogen bonding, the resonance of the conjugated system is disrupted and the bonds revert to a more unperturbed state. The skeletal distances in the ground-state enol, r(C2–C3) = 1.359 Å, r(C3–C4) = 1.443 Å, and r(C4–O4) = 1.262 Å, (see Section 5.5) become 1.304 ± 0.025 Å, 1.482 ± 0.023 Å, and 1.202 ± 0.017 Å, respectively, in the product radical where the hydrogen bond is severed and resonance stabilization is lost. Mean amplitudes of vibration were deduced to be consistent with a somewhat cold structure (265 K) in agreement with a previous finding[11] that a significant fraction of internal energy is released into translational motion of the fragments (note that the initial thermal energy here is higher than the temperature of the supersonic expansion[11]). The final refined theoretical and experimental $\Delta sM(s)$ and $\Delta f(r)$ curves are shown in Fig. 6-10. The theory and experiment match with χ^2 = 8.400 and R = 0.351. The polynomial background is also shown in order to illustrate the correction needed to set the data on the baseline. Interestingly, UED difference data in most other experiments have a flatter background than seen here. The "U" shaped curve needed in this experiment (in varying degrees at all time points) was attributed to the effects of laser scattering, but this remains speculative.

Using the refined product structure, its fractional contribution to each of the other time points may be obtained. Fig. 6-11 shows the experimental $\Delta sM(s)$ and $\Delta f(r)$ curves at time points ranging from +28 ps to +1273 ps (t_{ref} = –77 ps) along with the curves calculated for the refined product. The curves clearly show an increase in diffraction signal over time – compare these fit curves with the difference images shown in Figs. 6-1 and 6-2. An obvious observation is the low intensity of the +800 ps data

point. One possible explanation may be a problem with the translation stage that controlled the delay times in this experiment. A problem at the position corresponding to +800 ps delay may have caused a change in the beam path enough to affect the overlap between the three beams and reduce the signal. Because of the aberration and the relatively poor match with the refined theory, this point was eliminated from the calculation of the reaction time constant (see below).

Table 6-4. The fraction of the refined product at each time point

Delay time (ps)	Old program (Uedana)			New program (UED_2004)		
(t_{ref} = –77 ps)	fraction (%)	χ^2	*R*	fraction (%)	χ^2	*R*
–77	0	-	-	0	-	-
–27	0	-	-	0	-	-
+13	0.40 ± 1.82	4.257	9.479	0.40 ± 5.31	4.254	9.625
+18	0.06 ± 2.33	4.557	67.498	0.06 ± 5.29	4.557	71.291
+23	2.17 ± 1.79	4.390	1.730	2.19 ± 5.19	4.384	1.724
+28	1.70 ± 1.83	4.772	2.321	1.70 ± 5.22	4.775	2.333
+33	2.11 ± 1.81	4.590	1.813	2.13 ± 5.20	4.572	1.803
+43	2.85 ± 1.80	5.268	1.464	2.861 ± 5.31	5.268	1.464
+73	5.42 ± 1.78	6.021	0.816	5.44 ± 5.24	6.020	0.816
+98	4.11 ± 1.81	7.166	1.182	4.12 ± 5.32	7.155	1.183
+123	5.22 ± 1.85	7.193	0.952	5.25 ± 5.48	7.188	0.951
+173	6.89 ± 1.83	6.695	0.693	6.92 ± 5.44	6.684	0.692
+223	9.01 ± 1.82	6.711	0.530	9.04 ± 5.46	6.702	0.529
+423	12.69 ± 1.78	7.781	0.389	12.74 ± 5.24	7.732	0.388
+823	7.28 ± 1.80	5.884	0.599	7.31 ± 5.16	5.877	0.599
+1273	15.03 ± 1.87	7.781	0.343	15.09 ± 5.52	7.741	0.342

Error bars are 3σ. Uedana errors have been divided by $\sqrt{\chi^2 / \Delta range}$ (see Section 4.4.3).

The plot of the product fraction versus time is shown in Fig. 6-12. Using non-linear fitting of the single step reaction described in Section 4.6, a time constant (τ) of 247 ± 34 ps was obtained. To date, this is the slowest product rise studied by UED. Moving backwards slightly to Fig. 6-11, the $\Delta f(r)$ curves seem to show two distinct shapes before and after +400 ps delay. This and the slow reaction time suggest that a single step reaction may not be the best model for the formation of the OH loss products. However, and this is an issue often addressed in UED, the weaker overall signal at early

time points indicates that whatever the intermediate state, its structure is similar enough to the parent that its contribution is largely eliminated during reference-point subtraction. However, if an intermediate with a unique structure is present, then its contribution to the diffraction signal will be highlighted by astute choice of the reference time point for difference data creation. Fig. 6-13 schematically illustrates this point. Such methodology has been effective in past UED experiments involving intermediate structures.[12]

Alternative difference data were created for the +1273 ps time point using the +73 ps time point data as the reference. In a first-order reaction, the resulting data would be lower in amplitude yet still correspond to the parent→product reaction scheme. Conversely, if the reaction has multiple steps, the entire parent contribution will be removed. These data will then highlight information on the intermediate→product reaction. Fig. 6-14 shows the simulated $sM(s)$ and $f(r)$ curves for the structures of some possible intermediate states. The excited states shown all lie lower in energy than the excitation. The hot enol as an intermediate assumes that the fragmentation reaction occurs from S_0 after internal conversion. The other states assume various combinations of internal conversions and intersystem crossings. It's clear that the T_1 state is the only one that is completely structurally unique with a very different molecular scattering signature. S_2 also is fairly unique in that it achieves the fully delocalized C_{2v} structure that was not possible in the ground state. Although within the energy range possible in this experiment, the geometry optimization of T_2 suffered from convergence failure and the structure could not be obtained. The curves were calculated assuming 1000 K temperatures for the excited states and the T_B^{Max} (2256 K) for the hot parent.

Fig. 6-15 shows the fits (fractions and background optimized) of several of the excited state structures as possible intermediates with the (+1273 ps – +73 ps) alternate difference $\Delta sM(s)$ data. Although the elimination of OH from the T_1 ($\pi\pi^*$) state of acetylacetone has been suggested in the literature,[11] it does not match well as the intermediate structure in the UED experiment. The T_1 state possesses a non-planar structure with the C–O moiety twisted 66° out of the skeletal plane resulting in internuclear distances drastically different from S_0, particularly the indirect distances. Since the T_1 structure does not fit as the intermediate, a slow dissociation from T_1 is not the rate-determining step of this reaction.

Table 6-5. Tests of the possible intermediate structure

Structure	Fraction (%)	χ^2	R
S_0, 2256 K	–12.74 ± 4.40	4.976	0.594
S_1, 1000 K	–7.26 ± 2.51	7.084	0.747
S_2, 1000 K	–9.54 ± 3.41	4.457	0.560
T_1, 1000 K	–9.28 ± 3.71	9.983	1.115

The results of fraction and background optimization of several test cases for the intermediate structure using the alternate difference data are listed in Table 6-5. The plots of the $\Delta sM(s)$ and $\Delta f(r)$ curves corresponding to these results are shown in Fig. 6-15. Although a reasonable match to the data, the hot S_0 structure (after internal conversion) is discounted as the intermediate since reaction on the ground state surface would 1) be on a slower time scale and 2) favor the lowest energy pathway – here, both methyl loss and acetyl loss are lower in energy than OH loss. These behaviors are not consistent with the observed kinetics and structure. Additionally, the fractional contribution of the hot S_0 is not consistent with the fraction of intermediate expected at this time; in Table 6-4, by

subtracting the fraction of product at +73 ps from the fraction at +1273 ps (when the product fraction has leveled), one would expect –(15.09–5.44)% intermediate in the alternate difference data. Yet even disregarding this fact, the best intermediate structure fit is that of S_2, the ππ* state into which acetylacetone is excited by a photon of 266.7 nm radiation. However, the structureless absorption band[3,4,9] and absence of fluorescence[10,11] point toward a very short-lived S_2 state presumably depopulated by internal conversion. Consequently, the observed rise (the rate-determining step) is the intersystem crossing (ISC) from S_1 to T_1. A long lifetime of S_1 has also been observed for malonaldehyde.[13] T_1, then, dissociates in a time short enough that population does not build up and the structure is undetected by UED. It is not clear why the structure of S_1 does not appear in this alternate difference data although, but a speculation is that perhaps augmentation of S_1 by the close-lying S_2 is responsible for the "S_2" structure observed. Under this assumption, the appearance of pseudo-first-order behavior is consistent with ISC from S_1 being the rate-determining step for the overall elimination reaction. The structure of the intermediate could not be further refined with any accuracy due to the low signal/noise ratio of the alternate difference data.

The determined structures and the results of the calculations may be used to tentatively assign the reaction mechanism (see Fig. 6-16). Excitation at 266.7 nm populates the S_2 (ππ*) state. From here, ultrafast decay is most likely through internal conversion to S_1 (nπ*). Based on the rough determination of the intermediate structure the accepting state is likely a perturbed S_1, which then undergoes intersystem crossing to T_1 (ππ*) in 247 ps. The structure in the T_1 state is non-planar (C–O moiety twisted 66°

out of the skeletal plane), and as such, it promotes the cleavage of the OH radical in order to reform the double bond present in the product 3-penten-2-on-4-yl radical. Dominant Norrish-type cleavage reaction channels would be expected by a T_1 structure of $n\pi^*$ excitation.

6.4 Summary

Loss of OH from enolic acetylacetone is the dominant channel after 266 nm excitation and the structure of the product radical is deduced. The overall time constant for OH formation is determined to be 247 ± 34 ps. Furthermore, transient structures are found to precede the final product and are roughly identified to states in the excited singlet manifold. The influence of resonance stabilization on the molecular structure of the ground state, strengthened in the S_2 state, and weakened in S_1, is lost entirely in the T_1 state and the OH moiety is no longer co-planar with the conjugated bonds, aiding in efficient OH elimination. The $\pi\pi^*$ nature of the T_1 state facilitates reaction pathways that are not typical among ketones – OH-elimination from the β carbon as opposed to a Norrish Type-I cleavage. The absence of resonance stabilization results in the more "electron-localized" structure of the 3-penten-2-on-4-yl radical and the change in bond distances is directly observed.

6.5 References

[1] G. Gilli, F. Bellucci, V. Ferretti, and V. Bertolasi, J. Am. Chem. Soc. 111 (3), 1023 (1989); C. L. Perrin and J. B. Nielson, Annu. Rev. Phys. Chem. 48, 511 (1997).

[2] S. Xu, S. T. Park, J. S. Feenstra, R. Srinivasan, and A. H. Zewail, J. Phys. Chem. A 108 (32), 6650 (2004).

[3] K. N. Walzl, I. M. Xavier Jr., and A. Kuppermann, J. Chem. Phys. 86 (12), 6701 (1987).

[4] H. Nakanishi, H. Morita, and S. Nagakura, Bull. Chem. Soc. Jpn. 50 (9), 2255 (1977).

[5] P. Roubin, T. Chiavassa, P. Verlaque, L. Pizzala, and H. Bodot, Chem. Phys. Lett. 175 (6), 655 (1990).

[6] N. Nagashima, S. Kudoh, M. Takayanagi, and M. Nakata, J. Phys. Chem. A 105 (48), 10832 (2001).

[7] S. Coussan, C. Manca, Y. Ferro, and P. Roubin, Chem. Phys. Lett. 370, 118 (2003).

[8] D. Veierov, T. Bercovici, E. Fischer, Y. Mazur, and A. Yogev, J. Am. Chem. Soc. 99 (8), 2723 (1977).

[9] M.-C. Yoon, Y. S. Choi, and S. K. Kim, Chem. Phys. Lett. 300, 207 (1999).

[10] M.-C. Yoon, Y. S. Choi, and S. K. Kim, J. Chem. Phys. 110 (24), 11850 (1999).

[11] H. P. Upadhyaya, A. Kumar, and P. D. Naik, J. Chem. Phys. 118 (6), 2590 (2003).

[12] H. Ihee, B. M. Goodson, R. Srinivasan, V. A. Lobastov, and A. H. Zewail, J. Phys. Chem. A 106 (16), 4087 (2002).

[13] A. A. Arias, T. A. W. Wasserman, and P. H. Vaccaro, J. Chem. Phys. 107 (14), 5617 (1997).